ResearchGate

See discussions, stats, and author profiles for this publication at: https://www.researchgate.net/publication/223723340

Density functional theory study into the adsorption of CO2, H and CHx (x=0–3) as well as C2H4 on α-Mo2C(0001)

ARTICLE *in* SURFACE SCIENCE · JUNE 2006

Impact Factor: 1.93 · DOI: 10.1016/j.susc.2006.03.027

CITATIONS
29

READS
43

6 AUTHORS, INCLUDING:

Jun Ren
Chinese Academy of Sciences
282 PUBLICATIONS **6,852** CITATIONS
SEE PROFILE

Chun-Fang Huo
Chinese Academy of Sciences
46 PUBLICATIONS **725** CITATIONS
SEE PROFILE

Jianguo Wang
Northwestern Polytechnical University
208 PUBLICATIONS **3,264** CITATIONS
SEE PROFILE

Yong-Wang Li
Chinese Academy of Sciences
402 PUBLICATIONS **7,281** CITATIONS
SEE PROFILE

Available from: Yong-Wang Li
Retrieved on: 23 January 2016

Available online at www.sciencedirect.com
SCIENCE DIRECT
Surface Science 600 (2006) 2329–2337
SURFACE SCIENCE
www.elsevier.com/locate/susc

Density functional theory study into the adsorption of CO_2, H and CH_x ($x = 0$–3) as well as C_2H_4 on α-Mo_2C(0001)

Jun Ren [a], Chun-Fang Huo [a], Jianguo Wang [a,*], Zhi Cao [a], Yong-Wang Li [a], Haijun Jiao [a,b,*]

[a] State Key Laboratory of Coal Conversion, Institute of Coal Chemistry, Chinese Academy of Sciences, Taiyuan 030001, China
[b] Leibniz-Institut für Katalyse e.V. an der Universität Rostock, Albert-Einstein-Strasse 29a, 18059 Rostock, Germany

Received 7 December 2005; accepted for publication 22 March 2006
Available online 18 April 2006

Abstract

The structures and energetics of the chemisorbed CO_2, CH_x species and H as well as C_2H_4 on the α-Mo_2C(0001) surface have been computed at the GGA-RPBE level of density functional theory. It is found that CO_2 adsorbs dissociately into CO and O, in agreement with the experimental finding. The adsorbed O, CH_x and H species prefer the site of three surface molybdenum atoms over a second layer carbon atom (V_C site). On the basis of the calculated adsorption energies of CH_x and H, the sequential dehydrogenation of CH_4 and the C/C coupling reaction of CH_x have been discussed.
© 2006 Elsevier B.V. All rights reserved.

Keywords: DFT; CO_2 adsorption; CH_4 sequential dehydrogenation; Molybdenum carbides

1. Introduction

Transition metal carbides have attracted significant attentions due to their unique physical and chemical properties like extreme hardness, high melting points and metallic conductivity [1]. It has been demonstrated that transition metal carbides have excellent catalytic activity in a wide variety of hydrogen-involved reactions [2–11], such as hydrocarbon synthesis from CO hydrogenation [3,12–15], dehalogenation [8], hydrodesulfurization [16,17] and hydrodenitrogenation [18,19].

CH_4 dry reforming has received high attention, because it can convert these cheapest carbon containing materials into useful chemical products ($CH_4 + CO_2 = 2CO + 2H_2$). Supported group VIII noble metals like Ni, Pt, Ru and Rh are very active for this reaction at elevated temperatures, but have the problem of deactivation due to carbon deposition. Moreover, these metals are expensive and not available in large amounts [20]. The most frequently used commercial catalyst is the α-alumina supported nickel [21], but the problem is the deactivation caused by coke formation from CH_4 decomposition ($C + 2H_2$) and CO disproportionation ($C + CO_2$). Compared to steam reforming ($CH_4 + H_2O = CO + 3H_2$), CH_4 dry reforming has the advantages of producing synthesis gas at a low H_2/CO ratio, which is suitable for higher hydrocarbons in Fischer–Tropsch synthesis.

As an active catalyst for steam reforming, dry reforming and water gas shift ($H_2O + CO = CO_2 + H_2$), molybdenum carbides have attracted significant interest as potential substitutes for these precious noble metals and conventional nickel-based catalysts [22–26] due to their similar behaviors in surface catalysis [27]. In addition, a new catalytic application of molybdenum carbides has recently been established in the non-oxidative catalytic transformation of CH_4, e.g., MoO_3/ZSM-5 was proved to be the catalyst for benzene formation in this reaction [28–34]. Further studies revealed that MoO_3 is transformed into Mo_2C with CH_4 at

* Corresponding authors. Address: Leibniz-Institut für Katalyse e.V. an der Universität Rostock, Albert-Einstein-Strasse 29a, 18059 Rostock, Germany.
E-mail addresses: jgwang@sxicc.ac.cn (J. Wang), haijun.jiao@ifok-rostock.de (H. Jiao).

0039-6028/$ - see front matter © 2006 Elsevier B.V. All rights reserved.
doi:10.1016/j.susc.2006.03.027

high-temperature. It was found that Mo_2C in combination with ZSM-5 zeolite effectively catalyzes the aromatization of CH_4 with 80% selectivity at about 10–15% conversion [31–34]. Since this reaction has been observed neither on pure Mo_2C nor ZSM-5 alone, it was thought that the role of Mo_2C is the activation of CH_4 to yield CH_3 and CH_2 radicals with a certain lifetime on Mo_2C to couple into C_2H_4 [35]. The formed C_2H_4 can be oligomerized and aromatized on the acidic sites of ZSM-5. Under ultra-high-vacuum (UHV) condition it has been found that CH_3 and CH_2 radicals on Mo_2C/Mo(100) can combine into C_2H_4. Further works disclosed that Mo_2C/ZSM-5 is an active catalyst for the aromatization of the other lower alkanes, such as ethane [36], propane [37], *n*-butane and *iso*-butane [38].

Transition metal carbides are formed by substituting the lattice oxygen atoms of oxides by carbon atoms. The insertion of carbon atoms into Mo lattice causes the contraction of the d-band. Even with fewer electrons, the band is filled to a greater extent and the density of states at the Fermi level is close to those of the Group VIII noble metals [20,21], the center of d-band of which is closer to the Fermi level. Hammer and Nørskov [39] as well as others [40] have shown that the important surface parameters for the reactivity are the position of the whole d-bands relative to the Fermi level, which determines both the size of the bonding and anti-bonding energy shifts, and the degree of filling the anti-bonding states. Molybdenum carbides, in particular, are active and stable for hydrocarbon reforming and resistant to deactivation by SO_x poisoning or coking. Although these carbides exhibit a very good catalytic performance in these reactions, substantial fundamental understanding on catalytic nature and adsorption characters is not well established.

Over the past years, quantum chemical methods have become new tools for understanding the structures and stability as well as reactivity of active catalyst surfaces. With recent improvements in quantum chemistry, density functional theory methods (DFT) are capable of providing qualitative and, in many cases, quantitative insights into relationship between surface structures and catalytic activity. In this paper, we present a detailed DFT study of CO_2, H, CH_x ($x = 0$–3) species and C_2H_4 adsorption on α-Mo_2C(0001) in order to get the insight into their surface and structure properties.

2. Methods and models

All DFT calculations were carried out with the DMol^3 [41] program package in Materials Studio of Accelrys Inc. [42]. In DMol^3, the physical wave functions are expanded in terms of accurate numerical basis sets. We used the double-numeric quality basis set with polarization functions, and the semi-core pseudopotential was used for Mo atom [43]. The generalized gradient approximation (GGA) with the revised Perdew–Burke–Ernzerhof functional (RPBE) [44] was utilized. The RPBE functional usually gives absolute errors in adsorption energy of about 0.2 eV [44,45]. A Fermi smearing of 0.0005 a.u. (0.0136 eV) and a real-space cutoff of 5.5 Å were used to improve the computational performance. For numerical integration, the medium quality mesh was used, i.e. the convergence criteria for structure optimization and energy calculation were set to (1) SCF tolerance of 1×10^{-5} a.u./atom, (2) energy tolerance of 2.0×10^{-5} a.u./atom, (3) maximum force tolerance of 4.0×10^{-3} a.u./Å and (4) maximum displacement tolerance of 5.0×10^{-3} Å, respectively. Larger sets of k points were selected (4 or 16) for the case of the bulk α-Mo_2C(0001) surfaces, making sure that there is no significant change in the calculated energies when a larger number of k points was used. On the basis of CO_2 adsorption, we have tested different real-space cutoffs (5.5 Å vs. 6.0 Å), smearing values (0.0005 a.u. vs. Fermi level), and integration meshes (medium vs. fine). The differences in adsorption energy are 0.01, 0.008 and 0.06 eV, respectively. Therefore we used the real-space cutoffs of 5.5 Å and the smearing of 0.0005 a.u. as well as the medium quality meshes in our work. The complete linear synchronous transit and quadratic synchronous transit (LST/QST) method was used to locate the transition states. The validity of these methods has been proved [46].

A $p(2 \times 2)$ unit cell with a slab of four-layer thickness (2Mo + 2C) was used to describe these small molecules adsorption on α-Mo_2C(0001), corresponding to 1/4 ML coverage. The adsorbed species and the three top layers (2Mo + 1C) of α-Mo_2C(0001) were allowed to relax, while only the bottom layer (1C) was fixed at the calculated bulk lattice position in geometry optimization. In addition, for atomic H, and C as well as the open-shell molecular CH_x, the spin-unrestricted approach is used.

All geometrics were optimized without symmetry constraints. Adsorption energy is computed by subtracting the energies of the gas phase species and the surface from the energy of the adsorbed system as shown in Eq. (1): $E_{ads} = E(\text{adsorbate/slab}) - E(\text{adsorbate}) - E(\text{slab})$. With this definition, a negative E_{ads} corresponds to stable adsorption on the surface. For CH_4 dissociation into CH_x and H on the surface, the dissociation energy is defined as the difference between the sum of CH_x and H adsorption, and the sum of bare slab and free CH_4, $\Delta E_{diss} = [E(CH_x/\text{slab}) + (4 - x)E(H/\text{slab}) + xE(\text{slab})] - [E(CH_4) + 5E(\text{slab})]$, i.e.; negative ΔE_{diss} means exothermic dissociation, while positive ΔE_{diss} endothermic dissociation. Mulliken population analysis was carried out to estimate the partial charge on the adsorbed molecule or fragment for examining the qualitative trends in charge redistribution.

3. Results and discussion

3.1. Structure of α-Mo_2C

As a representative carbide phase, α-Mo_2C has an orthorhombic crystal structure with Mo atoms slightly distorted from their positions in close-packed planes and

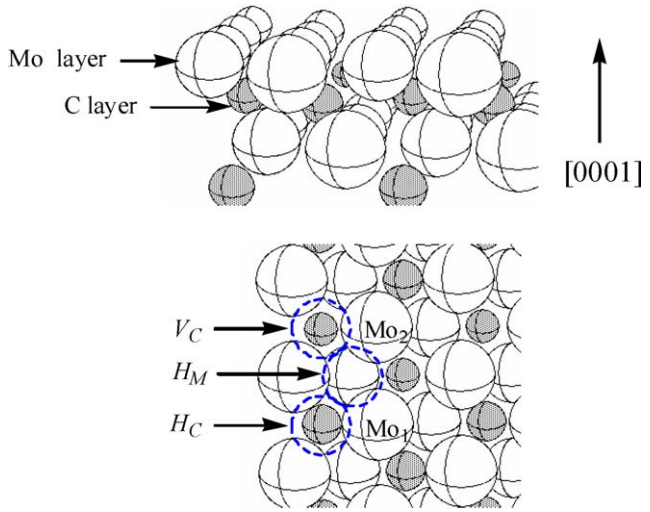

Fig. 1. Top and side views of the un-relaxed α-Mo_2C(0001). Mo_1 and Mo_2 indicate Mo atom coordination with two and one C atoms, respectively. White ball indicates Mo atoms, and gray ball denotes C atoms.

carbon atoms occupying ordered positions in lattice octahedral vacancies. This has resulted in many reports referring to the closest-packed surface as the (0001) surface [47]. In our previous work [48], the DFT calculated lattice constants for the bulk α-Mo_2C ($a = 4.748$ Å, $b = 6.026$ Å and $c = 5.204$ Å) are close to the experimental values ($a = 4.729$ Å, $b = 6.028$ Å and $c = 5.197$ Å) [47]. The structure of α-Mo_2C perpendicular to the [0001] direction includes a series of alternating Mo and C atom layers. As shown in Fig. 1, there are two individual Mo atoms (Mo_1 and Mo_2) with different carbon coordination numbers on the Mo-terminated surface. Mo_1 coordinates with two carbon atoms of the sublayer and Mo_2 coordinates with one carbon atom of the sublayer. In comparison with the bulk Mo atom, Mo_1 has one coordination vacancy and Mo_2 has two coordination vacancies. Our focus is the Mo-terminated site, which is very important for the catalytic activity and the catalytic reactions occur mainly on it [16–19]. In our previous work [48], we have found that the C-terminated surface has also activity for oxygen and CO adsorption, but their adsorption energies (−5.36 and −1.74 eV) are much lower than those on the Mo-terminated surface (−8.46 and −2.23 eV). In addition, the computed CO_2 adsorption energy on the C-terminated surface ($p(2 \times 2)$ super cell) of −0.12 eV is lower than that (−2.38 eV) on the Mo-terminated surface. So the C-terminated surface is not considered in present work.

3.2. CO_2 adsorption on α-Mo_2C(0001)

As shown in Fig. 1, there are three different three-fold hollow sites on the Mo-terminated surface for adsorption: (i) three surface Mo atoms over a second layer carbon atom (V_C site), (ii) three surface Mo atoms over a second layer Mo atom (H_M site), (iii) three surface Mo atoms over a first layer carbon atom (H_C site), respectively. The possible top and bridge sites were also considered. All initial orientations on different sites of α-Mo_2C(0001) were considered, but only five structures (**1**–**5**) of chemisorbed CO_2 at 1/4 ML coverage were found as stable surface forms, as shown in Fig. 2. The calculated adsorption energies and bond parameters as well as the net charges of the chemisorbed CO_2 on α-Mo_2C(0001) are listed in Table 1.

As given in Table 1, **1** is the most stable adsorbed surface structure with the largest adsorption energy (−2.38 eV), while **2**–**5** have much lower adsorption energies

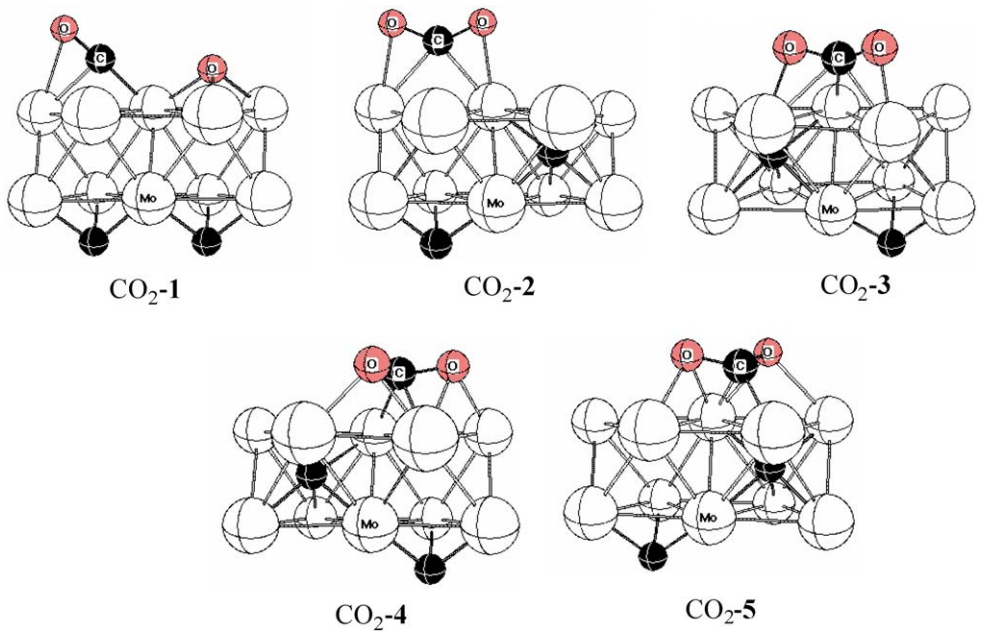

Fig. 2. Surface structures of CO_2 adsorption on the Mo-terminated α-Mo_2C(0001).

Table 1
The calculated geometric parameters (d, Å and θ, degree), adsorption energies (E_{ads}, eV) and the net charge (q) of CO_2 on α-Mo_2C(0001)

	E_{ads}	d_{O-C}	d_{C-Mo}	d_{O-Mo}	$\theta(O_1CO_2)$	q
CO_2–**1**	−2.38	1.233	1.997, 2.281	1.993–2.109	144.06	−1.014[a]
CO_2–**2**	−0.54	1.250, 1.264	2.249, 2.341	2.254, 2.288	135.09	−0.291
CO_2–**3**	−0.45	1.363, 1.312	2.185, 2.388	2.059, 2.166	117.57	−0.557
CO_2–**4**	−0.16	1.368, 1.371	2.108, 2.196	2.273, 2.328	112.03	−0.635
CO_2–**5**	−0.14	1.355, 1.367	2.172, 2.255	2.288, 2.291	111.84	−0.589
CO_2		1.179			180.00	0.0

[a] The sum of adsorbed CO (−0.285) and O (−0.729).

(−0.54 to −0.14 eV). In **1**, CO_2 dissociates spontaneously into CO and O during optimization. The formed O atom locates at the V_C site and forms three Mo–O bonds with an averaged length of 2.051 Å. The formed CO bridges two adjacent Mo of V_C site and the C=O bond is elongated compared with free CO_2 (1.233 Å vs. 1.179 Å). This result agrees very well with the experimental finding that CO_2 dissociates on Mo_2C, and the formed atomic oxygen migrates into the bulk and the CO is desorbed during temperature-programmed desorption (TPD) [25,49], leaving a coordinatively unsaturated site available for another CO_2 coordination. In our previous work [48], on the Mo-terminated surface, both CO and O also prefer to chemisorb on the V_C sites with chemisorption energies of −2.23 and −4.39 eV (relative to O_2/2), respectively. The rather lower chemisorption energy of CO compared to atomic oxygen confirms the TPD observation.

For **2**–**5**, CO_2 adsorbs activated but not dissociated. In **2** (V_C sites), CO_2 interacts with two adjacent Mo atoms via two C=O bonds and forms two Mo–C bonds, and the C–O bonds are elongated to 1.250 and 1.264 Å. In **3**, CO_2 interacts with three Mo atoms on the surface by occupying one H_M site and the carbon center caps three Mo atoms with the formation of three Mo–C bonds, and each of the oxygen atoms interacts with the adjacent Mo atom, and the C–O bonds are elongated to 1.312 and 1.363 Å. In **4**, CO_2 interacts with four Mo atoms by occupying one H_M site and one V_C site, and the carbon center bridges the adjacent Mo atoms to form two Mo–C bonds. Each of oxygen of CO_2 in **4** interacts with two surface Mo atoms, and the C–O bonds are elongated to 1.368 and 1.371 Å. In **5**, CO_2 located on one H_M site and one H_C site. Each of oxygen in CO_2 in **5** interacts with two surface Mo atoms and the C–O bonds are elongated to 1.355 and 1.367 Å. For **2**–**5**, the adsorbed CO_2 moiety has bent structure with an OCO angle of about 111°.

Apart from the structures and energies, it is also interesting to look into the change of the charges of CO_2. The net charges of the chemisorbed CO_2 on α-Mo_2C(0001) are given in Table 1, compared with those of free CO_2. It clearly shows that the chemisorbed CO_2 molecules are partially negative charged (−0.589 for **5** to −0.291 for **2**), indicating the electron transfer from the α-Mo_2C(0001) surface into CO_2. The same phenomena are found for chemisorbed CO_2 on Ni surfaces [50]. Freund and Messmer [51] suggested that the bending mechanism of the partially negative charged $CO_2^{\delta-}$ is due to the effect of electrons transfer from surface into the anti-bonding orbital of CO_2. Therefore the best and most appropriated description of CO_2 on the surface should be $CO_2^{\delta-}$.

Generally CO_2 activation on transition metal surfaces is structure sensitive, i.e.; different surface has different activation. For example, CO_2 adsorbs dissociatively on Fe(111), Fe(100) and Ni(110), but non-dissociativly on Fe(100) and Ni(111), while dissociativly and non-dissociativly on Ni(100) [50]. It also showed that CO_2 adsorbs dissociatively on clean Mo(100) [52] and polycrystalline Mo [53] at the lower temperature. It was believed that on Ni(110), Ni(100) and Fe(111) the chemisorbed $CO_2^{\delta-}$ anionic species represents an intrinsic precursor for CO_2 dissociation into CO and atomic oxygen [54,55]. Nassir and Dwyer [56] found that CO_2 is strongly chemisorbed on Fe(100) and undergoes sequential C–O bond cleavage, and proposed that CO_2 dissociates in two steps with an intermediate complex composed of atomic oxygen and π-bonded CO. Choe et al. [55] calculated the structures of the reaction intermediates, using the first CO bond breaking in carbon dioxide on Pt(111) and Fe(111), and the reaction intermediate complex is regarded as a possible intermediate complex model, which is formed in a CO oxidation reaction.

3.3. CH_x and H adsorption on α-Mo_2C(0001)

CH_4 decomposition on the surface results in the formation of CH_x ($x = 0$–3) and adsorbed hydrogen, so the adsorption energies of the dissociated species bear an essential implication in CH_4 dissociation. Now we analyze the adsorption of CH_x species and H on α-Mo_2C(0001).

For CH_3, the top, bridge and 3-fold hollow adsorption sites are considered. As shown in Fig. 3, there are only three favorable adsorption structures on α-Mo_2C(0001), CH_3(V_C) **6**, CH_3(H_M) **7** and CH_3(H_C) **8**. In **6**–**8**, CH_3 has a η^3 capping model with three surface Mo atoms at different active sites (V_C, H_M, and H_C site), and the three C–H bonds point to the nearest neighbor atoms in favor of the eclipsed conformation. The calculated structural and energetic parameters are listed in Table 2.

In **6**, the carbon atom is 1.506 Å above the surface and the C–Mo distances are 2.331, 2.401 and 2.405 Å, respectively. In **7**, the carbon atom is located 1.508 Å above the surface and C–Mo distances are 2.382, 2.419 and

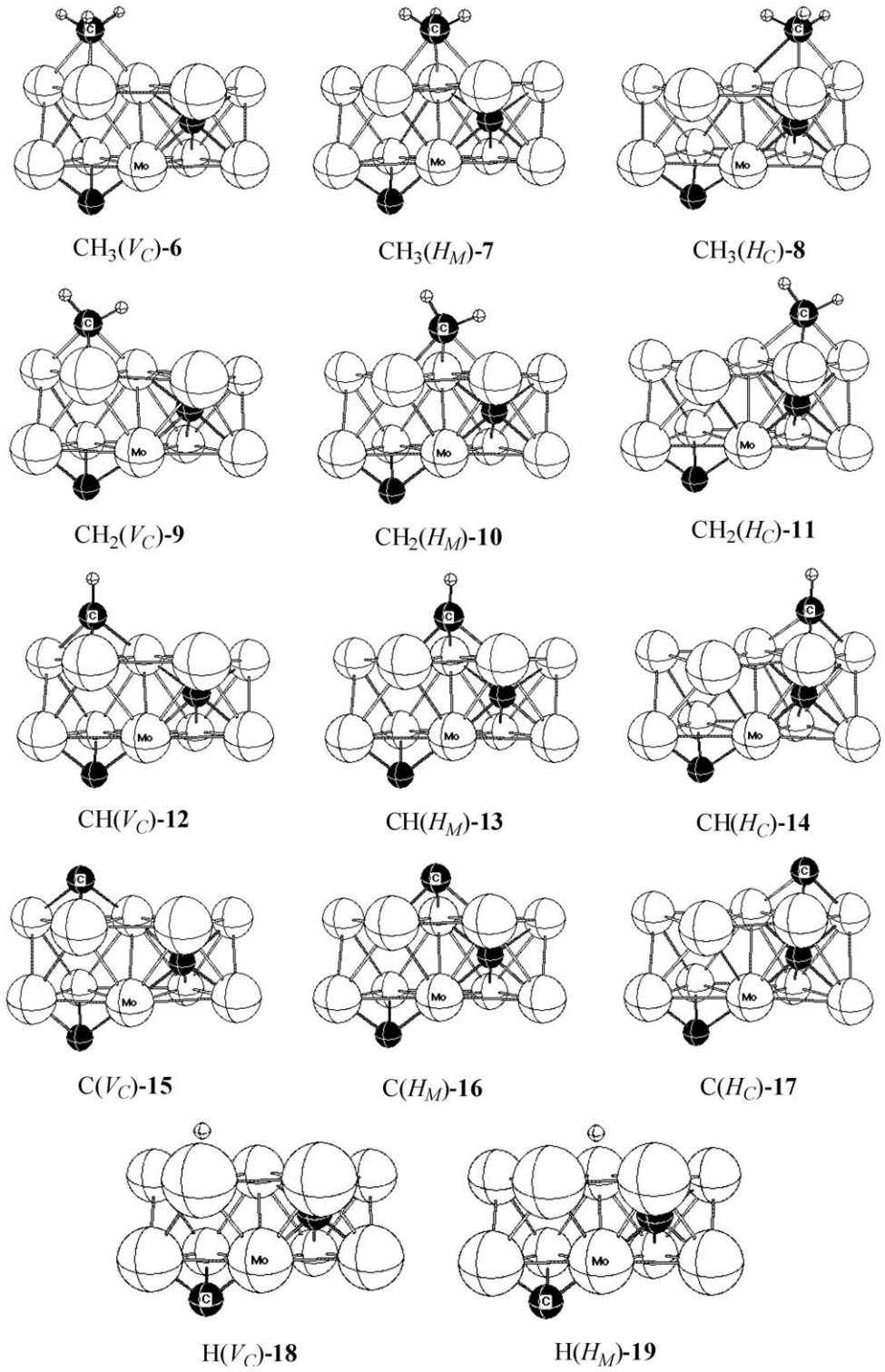

Fig. 3. Surface structures of CH_x species adsorption on the Mo-terminated α-Mo_2C(0001).

2.454 Å, respectively. In **8**, the carbon atom is 1.509 Å above the surface, and C–Mo distances are 2.365, 2.465 and 2.625 Å, respectively. As given in Table 3, **6** is the most stable structure for CH_3 adsorption on α-Mo_2C(0001) with a chemisorption energy of −2.37 eV, while **7** and **8** are less stable than **6** by about 0.34 and 0.50 eV, respectively.

Alike CH_3, CH_2 also has three stable adsorption structures $CH_2(V_C)$ **9**, $CH_2(H_M)$ **10**, and $CH_2(H_C)$ **11**, as shown in Fig. 3. In **9**, one H atom near the top site has a C–H bond length of 1.131 Å, while the other H atom pointing midway between two neighboring Mo atoms has a C–H bond of 1.086 Å. In addition, the H–C–H angle is reduced from 135° of the isolated CH_2 radical to 101.9°. In **10** and

Table 2
The calculated geometric parameters (d, Å and θ, degree), chemisorption energies (E_{ads}, eV) and charges (q, e) of CH_x and H chemisorbed on α-$Mo_2C(0001)$

Adsorbate	E_{ads}	d_{Mo-C} (d_{H-Mo})	d_{C-H}	θ_{HCH}	q
CH_3 (doublet)			1.082	120.0	
$CH_3(V_C)$–**6**	−2.37	2.331, 2.401, 2.405	1.100, 1.101, 1.102	104.1, 104.5, 104.7	−0.065
$CH_3(H_M)$–**7**	−2.03	2.382, 2.454, 2.419	1.094, 1.109, 1.100	103.5, 104.7, 104.8	−0.046
$CH_3(H_C)$–**8**	−1.87	2.365, 2.465, 2.625	1.090, 1.097, 1.109	104.1, 104.6, 105.7	−0.053
CH_2 (triplet)			1.081	135.5	
$CH_2(V_C)$–**9**	−4.37	2.156, 2.215, 2.252	1.086, 1.131	101.9	−0.309
$CH_2(H_M)$–**10**	−4.19	2.173, 2.238, 2.255	1.083, 1.146	98.9	−0.237
$CH_2(H_C)$–**11**	−3.84	2.161, 2.227, 2.416	1.084, 1.132	101.6	−0.220
CH (doublet)			1.120		
$CH(V_C)$–**12**	−6.61	2.039, 2.094, 2.202	1.089		−0.482
$CH(H_M)$–**13**	−6.44	2.060, 2.120, 2.176	1.085		−0.409
$CH(H_C)$–**14**	−6.05	2.097, 2.102, 2.222	1.085		−0.370
$C(V_C)$–**15**	−7.25	1.964, 2.005, 2.041			−0.534
$C(H_M)$–**16**	−6.98	2.013, 2.022, 2.033			−0.437
$C(H_C)$–**17**	−6.30	2.013, 2.058, 2.088			−0.416
$H(V_C)$–**18**	−3.09 (−0.81)[a]	1.971, 2.016, 2.023			−0.106
$H(H_M)$–**19**	−2.96 (−0.67)[a]	1.998, 2.059, 2.084			−0.052

[a] The chemisorption energy of H relative to $1/2H_2$, $E_{ads}(H) = E(H/slab) - [1/2E(H_2) + E(slab)]$.

Table 3
The calculated geometric parameters (d, and Å), adsorption energies (E_{ads}, eV) and charges (q, e) of C and H of ethylene on α-$Mo_2C(0001)$

Adsorbate	E_{ads}	d(C–Mo)	d(C–H)	d(C–C)	q(C)	q (H)
Eth(H_M)–**20**	−1.13	2.301, 2.274 2.476, 2.511	1.08–1.110	1.474	−0.311,−0.338	0.154–0.172
Eth-Tilited (V_C)–**21**	−1.02	2.335, 2.339 2.429, 2.392	1.076–1.119	1.465	−0.245, −0.426	0.141–0.186
Eth(V_C)–**22**	−0.91	2.302, 2.314 2.443, 2.477	1.076–1.120	1.445	−0.286, 0.289	0.154–0.169
Eth(H_M)–**23**	−0.89	2.262, 2.256 2.447, 2.524	1.077–1.113	1.454	−0.298, −0.300	0.151–0.165
C_2H_4			1.094	1.342	−0.168, −0.168	0.084, 0.084

11, the H atom near the top site has C–H bond length of 1.146 and 1.132 Å, respectively, and the H–C–H angles are 98.9° and 101.6°. As given in Table 2, **9** is the most stable structure for CH_2 adsorption with chemisorption energy of −4.37 eV, while **10** and **11** are less stable than **9** by 0.18 and 0.53 eV, respectively. It is to note that CH_2 adsorption is about two times stronger than CH_3 on the same site.

For CH adsorption, there are also three stable structures $CH(V_C)$ **12**, $CH(H_M)$ **13** and $CH(H_C)$ **14**, as shown in Fig. 3. In all cases, the C–H bond is almost perpendicular to the Mo-terminated α-$Mo_2C(0001)$ surface. The most stable adsorption structure is **12** with an adsorption energy of −6.61 eV, while **13** and **14** are less stable (−6.44 and −6.05 eV, respectively). It is to note that CH adsorption is about three times stronger than CH_3 on the same surface.

For carbon atom, only three stable adsorption structures are found, $C(V_C)$ **15**, $C(H_M)$ **16** and $C(H_C)$ **17**. The most stable adsorption structure is **15** with an adsorption energy of −7.25 eV, while **16** and **17** are less stable (−6.98 and −6.30 eV, respectively). Thus, carbon atom prefers to the V_C site, which is similar to C-terminated α-$Mo_2C(0001)$ surface [57].

In addition, the adsorption of H atom on α-$Mo_2C(0001)$ was investigated. All possible adsorption sites on the Mo-terminated surface were considered. Adsorption on the top and bridge sites did not exist during optimization structures. The adsorption energies are listed in Table 2. It is found that H atom adsorbs more strongly on the V_C site ($H(V_C)$ **18**) than on the H_M site ($H(H_M)$ **19**) with an adsorption energy of −0.81 and −0.67 eV, respectively. It is interesting to note that H atom is unstable on the H_C site with a C atom directly below them. During structure optimization, the H atom spontaneously shifts from the H_C site to H_M or V_C site. One might expect that H atom could occupy the H_C site at higher coverage, but this is beyond the scope of this study.

The most stable adsorption site determined for CH_x ($x = 0$–3) chemisorption on α-$Mo_2C(0001)$ is the V_C site. Adsorption on the surface results in a net transfer of electrons to the adsorbate in all cases, the magnitude of which decrease with a decrease in the valence of the species. For

example, the net charge of CH is −0.482 on the adsorbate, while those of CH_2 and CH_3 are −0.309 and −0.065, respectively. This trend may be related to the increased population of the adsorbate valence orbitals, which are involved in the formation of the adsorbate–substrate bond [20b].

3.4. CH_4 sequential dehydrogenation

In gas phase, CH_4 sequential dehydrogenation is highly endothermic, and the computed energies are 4.68, 4.89, 4.67 and 3.66 eV for each step, which means that a total of 17.90 eV is needed for the complete dehydrogenation. On the basis of the calculated most stable CH_x ($x = 0$–3) species and H atom on α-Mo_2C(0001), the energy scheme of dehydrogenation is shown in Fig. 4. On α-Mo_2C(0001), there is significant reduction in the dissociation energy, owing to the presence of the strong Mo–CH_x and Mo–H bonds. It is to note that all individual steps are endothermic, and CH_4 dissociation into CH_3 and H is the most difficult step (0.73 eV), and the total reaction energies of CH_4 complete dehydrogenation is 1.67 eV. Therefore, a complete dissociation of CH_4 into surface C and H is very hard. Due to their importance in Fischer–Tropsch synthesis, the structure and stability of the surface species CH_3 have been studied intensively by means of theoretical and experimental methods, and CH has been identified as the most stable intermediate on the Pt metals surface [20]. On α-Mo_2C(0001), however, adsorbed carbon is the most stable surface species as indicated by the calculated adsorption energy in Table 2.

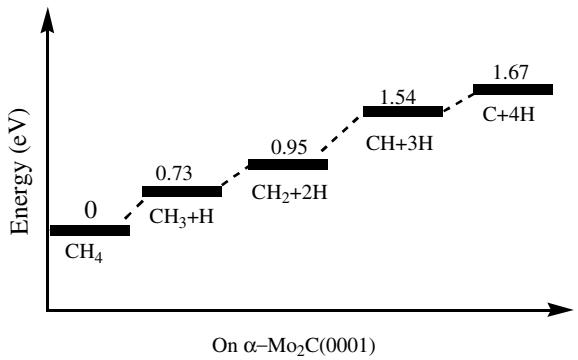

Fig. 4. Thermodynamic energetic scheme of CH_4 sequential dehydrogenation system.

3.5. C_2H_4 adsorption on α-Mo_2C(0001)

As an intermediate for the direct conversion of CH_4 into benzene, ethylene is investigated. The exact knowledge of the adsorption mode of ethylene on transition metal surfaces is of importance for the understanding of catalytic reactions involving this small olefin. Numerous experimental studies of the adsorption of ethylene on a variety of transition metal surfaces have been reported. The calculated structures and energies of ethylene adsorption on Mo-terminated α-Mo_2C(0001) are given in Fig. 5 and Table 3, respectively.

In **20**, ethylene locates in the H_M site which is adjacent to two V_C sites with C–C bond length of 1.474 Å, and the C–C bond is slightly elongated by 0.132 Å compared with free ethylene. The optimized C–H bonds are bent away from the surface plane by 45.8°. In **21**, ethylene adsorbs aslant at the V_C site, which is oriented with its C–C axis on average at an angle of 47.1° of Mo-terminated α-Mo_2C(0001) and the computed C–C bond length is 1.465 Å. In **22** and **23**, ethylene adsorbs at the V_C site adjacent to two H_M sites and at the H_M site adjacent to two H_C sites. The C–C bond lengths to free ethylene are elongated about 0.102 and 0.108Å, respectively. On α-Mo_2C(0001), **20** is the most stable adsorbed structure on the Mo hollow site (H_M site, −1.13 eV), while **21**, **22** and **23** are higher in energy (−1.02, −0.91, and −0.89 eV, respectively).

3.6. CH_x coupling reaction on α-Mo_2C(0001)

It has long been believed that alkyl chain growth in Fischer–Tropsch catalysis on metal surfaces proceeds by CH_x (C/C) coupling [58]. The prototypical C/C coupling

Table 4
Calculated barriers (E_a) and reaction energies (ΔE_r) for C/C coupling on α-Mo_2C(0001)

Coupling reaction	E_a (eV)	ΔE_r (eV)
$CH_3 + CH_3 \rightarrow CH_3CH_3$	4.28	0.87
$CH_3 + CH \rightarrow CH_3CH$	2.13	0.77
$CH_3 + CH_2 \rightarrow CH_3CH_2$	1.89	0.49
$CH_2 + CH_2 \rightarrow CH_2CH_2$	1.31	0.17
$CH_2 + CH \rightarrow CH_2CH$	0.97	−0.25
$CH + CH \rightarrow HCCH$	1.01	−0.32

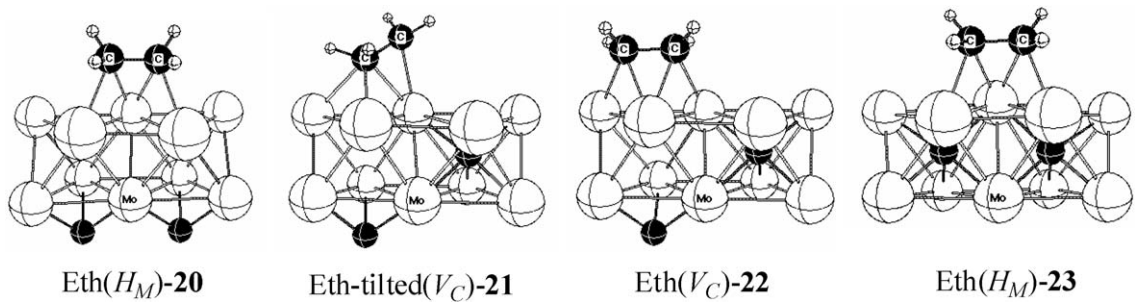

Fig. 5. Surface structures of ethylene adsorption the Mo-terminated α-Mo_2C(0001).

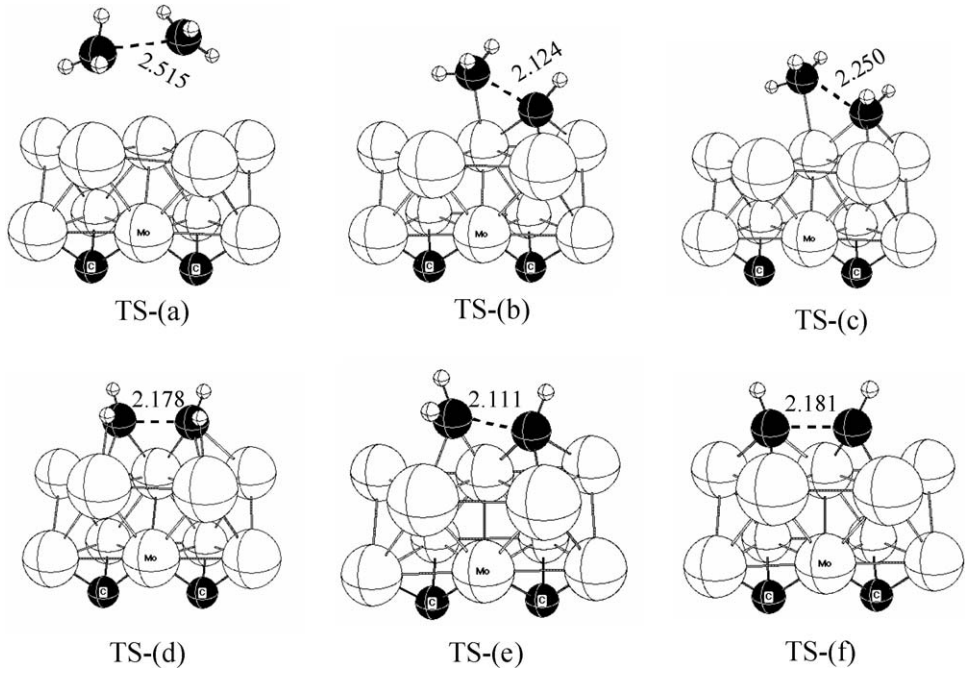

Fig. 6. Structures of transition state for C/C coupling reaction: (a) CH_3/CH_3, (b) CH_3/CH, (c) CH_3/CH_2, (d) CH_2/CH_2, (e) CH_2/CH and (f) CH/CH.

reaction has many possibilities: CH/CH, CH/CH_2, CH/CH_3, CH_2/CH_2, CH_2/CH_3 and CH_3/CH_3. The calculated C/C coupling barriers (E_a) and reaction energies (ΔE_r) are given in Table 4. It is clearly to see that all the C/C coupling reactions are disfavored. The highest barrier is found for CH_3/CH_3 (4.28 eV), and this is associated with the valence of the adsorbed radical on the surface. On the basis of CH_3, CH_2, and CH adsorption, we have studied the adsorbate–adsorbate interaction at the increased coverage by comparing the adsorption energies of these species at the 1/2 ML and 1/4 ML. For the most stable adsorption site (V_C site), the adsorption energy differences between 1/2 ML and 1/4 ML are 0.03 eV for CH_3, 0.09 eV for CH_2, and 0.07 eV for CH. These results indicate that adsorbed species at the 1/2 ML show relatively weak lateral repulsion (see Fig. 6).

Our calculation shows that CH_3 is an unfavorable species for C/C coupling with high barriers (the activation energies are 4.28, 2.13 and 1.89 eV for CH_3/CH_3, CH_3/CH and CH_3/CH_2, respectively), and this is consistent with the work of others [58b]. CH_2/CH_2 coupling is also unfavorable with an activation energy of 1.31 eV to yield adsorbed ethylene. In addition, CH/CH and CH/CH_2 couplings have rather lower barriers (1.01 and 0.97 eV, respectively), and they are kinetically competitive. Compared to CH_2/CH_2 coupling to form ethylene, CH/CH_2 coupling to form adsorbed vinyl radical has lower barrier (1.31 vs. 0.97 eV). This suggests that direct CH_2/CH_2 coupling should be less possible at low coverage. Furthermore that lower barrier of CH/CH coupling to form acetylene on the surface shows the special role of CH, which might be directly associated with the aromatization process of CH_4. A recent experimental work [59] also concluded that the principal route for the aromatization of CH_4 is the formation of C_2H_2 over Mo_2C and the role of ZSM-5 is very likely to promote the reactions of C_2H_2 (oligomerization and aromatization) migrated from Mo_2C into ZSM-5.

4. Conclusion

The adsorption behaviors of CO_2, CH_x species, H and C_2H_4 on α-$Mo_2C(0001)$ were investigated at the GGA-RPBE level of density functional theory. The main subjective of this study is the structures and energetics of the adsorbed surface species, which are directly associated with the mechanism of Fischer–Tropsch synthesis. In agreement with the experimental observation, CO_2 dissociates spontaneously on the Mo surface, and the formed O locates at three surface Mo atoms over a second layer carbons atom (V_C site), and the formed CO bridges two surface Mo atoms of the V_C site. Other adsorption structures have only activated CO_2 and are less stable.

Energetically, the CH_x species and atomic H adsorb strongly at the preferred site (V_C site), which are similarly to oxygen adsorption on the same surface. The chemisorption energy of CH_x increases with their increasing number of the valence orbitals in the order of $CH_3 < CH_2 < CH < C$. Compared with gas-phase CH_4 dissociation, adsorbed CH_4 has much lower, but still endothermic dehydrogenation energies.

Furthermore, the C/C coupling of the adsorbed CH_x species has also been computed. The calculated activation energy decreases with the increasing number of the valence orbitals. The low activation energies of the CH/CH, CH_2/CH and CH_2/CH_2 coupling reactions might reveal the role of the surface C_2H_2, CH_2CH and C_2H_4, which might be

directly associated with the aromatization process of CH_4 or other lower alkanes.

Acknowledgements

This work has been supported by the National Nature Science Foundation of China (20473111, 20590360 and 20573127).

References

[1] Y. Kumashiro, Electric Refractory Materials, Marel Dekker, New York, 2000.
[2] S.T. Oyama, Catal. Today 15 (1992) 1979.
[3] I. Kojima, E. Miyazaki, J. Catal. 89 (1984) 168.
[4] J.S. Lee, K.H. Lee, J.Y. Lee, J. Phys. Chem. 96 (1992) 362.
[5] T.P.St. Clair, S.T. Oyama, D.F. Cox, Surf. Sci. 511 (2002) 294.
[6] L. Bugyi, A. Oszkó, F. Solymosi, Surf. Sci. 519 (2002) 139.
[7] B. Dhandapani, T.P.St. Clair, S.T. Oyama, Appl. Catal. A: Gen. 168 (1998) 219.
[8] B. Dhandapani, S.T. Oyama, Catal. Lett. 35 (1995) 353.
[9] M. Orita, I. Kojima, E. Miyazaki, Bull. Chem. Soc. Jpn. 59 (1986) 689.
[10] C. Pham-Huu, M.J. Ledoux, J. Guille, J. Catal. 143 (1993) 249.
[11] H.H. Hwu, J.G.G. Chen, Chem. Rev. 105 (2005) 185.
[12] M. Saito, R.B. Anderson, J. Catal. 63 (1980) 438.
[13] M. Logan, A. Gellman, G.A. Somorjai, J. Catal. 94 (1985) 60.
[14] G.S. Ranhotra, A.T. Bell, J.A. Reimer, J. Catal. 108 (1987) 40.
[15] J.S. Lee, M.H. Yeom, D.-S. Lee, J. Mol. Catal. A 62 (1990) L45.
[16] S.T. Oyama, C.C. Yu, S. Ramanathan, J. Catal. 184 (1999) 535.
[17] J.A. Rodriguez, J. Dvorak, T. Jirsk, Surf. Sci. 457 (2000) L413.
[18] T.E. Lucy, T.P.St. Clair, S.T. Oyama, J. Mater. Res. 13 (1998) 2321.
[19] V. Schwartz, V.T. Da Silva, S.T. Oyama, J. Mol. Catal. A 163 (2000) 251.
[20] (a) J. Haber, E. Lalik, Catal. Today 33 (1997) 119;
(b) M.A. Peterson, S.J. Jenkins, D.A. King, J. Phys. Chem. B 105 (2004) 5909;
(c) F. Solymosi, in: E.G. Derouane (Ed.), Catalytic Activation and Functionalisation of Light Alkanes, Kluwer Academic Publishing, Netherlands, 1998, p. 369;
(d) C. Zheng, Y. Apeloig, R. Hoffmann, J. Am. Chem. Soc. 110 (1988) 749;
(e) M.L. Turner, P.K. Byers, H.C. Long, P.M. Maitlis, J. Am. Chem. Soc. 115 (1993) 4417.
[21] D.L. Trimm, Catal. Today 49 (1999) 3.
[22] J.B. Claridge, A.P.E. York, A.J. Bruggs, C. M-Alvares, J. Sloan, S.C. Tsang, M.L.H. Green, J. Catal. 189 (1998) 85.
[23] Y. Tsuji, T. Miyao, S. Naito, Catal. Lett. 69 (2000) 195.
[24] S. Naito, M. Tsuji, T. Miyao, Catal. Today 77 (2002) 161.
[25] D.C. LaMont, W.J. Thomson, Chem. Eng. Sci. 60 (2005) 3553.
[26] J. Sehested, C.J.H. Jacobsen, S. Rokni, J.R.R. Nielsen, J. Catal. 201 (2001) 206.
[27] R.B. Levy, M. Boudart, Science 181 (1973) 547.
[28] L. Wang, L. Tao, M. Xie, G. Xu, J. Huang, Y. Xu, Catal. Lett. 21 (1993) 35.
[29] F. Solymosi, A. Erdőhelyi, A. Szőke, Catal. Lett. 32 (1995) 43.
[30] Y. Xu, S. Liu, L. Wang, M. Xie, X. Guo, Catal. Lett. 30 (1995) 135.
[31] F. Solymosi, J. Cserényi, A. Szőke, T. Bánsági, A. Oszkó, J. Catal. 165 (1997) 150.
[32] A. Szőke, F. Solymosi, Appl. Catal. A: Gen. 142 (1996) 361.
[33] D. Wang, J.H. Lunsford, M.P. Rosynek, Topics Catal. 2 (1996) 299.
[34] F. Solymosi, A. Szőke, J. Cserényi, Catal. Lett. 39 (1996) 157.
[35] J. Raskó, J. Kiss, Appl. Catal. A: Gen. 253 (2003) 427.
[36] F. Solymosi, A. Szóke, Appl. Catal. A: Gen. 166 (1998) 225.
[37] F. Solymosi, R. Németh, L. Óvári, L. Egri, J. Catal. 195 (2000) 316.
[38] (a) S. Yuan, S.B. Derouane-Abd Hamid, Y. Li, P. Ying, Q. Xin, E.G. Derouane, C. Li, J. Mol. Catal. A 180 (2002) 245;
(b) F. Solymosi, R. Németh, A. Széchenyi, Catal. Lett. 82 (2002) 213;
(c) F. Solymosi, A. Széchenyi, J. Catal. 223 (2004) 221.
[39] B. Hammer, J.K. Nørskov, Surf. Sci. 343 (1995) 211.
[40] Venkataraman Pallassanam, Matthew Neurock, J. Catal. 191 (2000) 301.
[41] (a) B. Delley, J. Chem. Phys. 92 (1990) 508;
(b) B. Delley, J. Phys. Chem. 100 (1996) 6107;
(c) B. Delley, J. Chem. Phys. 113 (2000) 7756.
[42] (a) M.C. Payne, D.C. Allan, T.A. Arias, J.D. Joannopoulos, Rev. Mod. Phys. 64 (1992) 1045;
(b) V. Milman, B. Winkler, J.A. White, C.J. Pickard, M.C. Payne, E.V. Akhmataskaya, R.H. Nobes, Int. J. Quantum Chem. 77 (2000) 895.
[43] B. Delley, Phys. Rev. B 66 (2002) 15525.
[44] B. Hammer, L.B. Hansen, J.K. Nørskov, Phys. Rev. B 59 (1999) 7413.
[45] P. Liu, J.A. Rodrigues, J.T. Muckerman, J. Phys. Chem. B 108 (2004) 15662.
[46] M. Sun, A.E. Nelson, J. Adjaye, J. Catal. 233 (2005) 411.
[47] (a) E. Parthe, V. Sadagopan, Acta Crystallogr. 16 (1963) 202;
(b) S. Otani, Y. Ishizawa, J. Cryst. Growth. 154 (1995) 202.
[48] J. Ren, C.-F. Huo, J.-G. Wand, Y.-W. Li, H. Jiao, Surf. Sci. 596 (2005) 212.
[49] M. Nagai, K. Oshikawa, T. Kurakami, T. Miyao, J. Catal. 180 (1998) 14.
[50] S.-G. Wang, D.-B. Cao, Y.-W. Li, J.-G. Wang, H. Jiao, J. Phys. Chem. B 109 (2005) 18956.
[51] H.-J. Freund, R.P. Messmer, Surf. Sci. Lett. 172 (1986) A333.
[52] B.W. Walker, P.C. Stair, Surf. Sci. 91 (1980) L40.
[53] L.D. López-Carreño, J.M. Heras, L. Viscido, Surf. Sci. 377–379 (1997) 615.
[54] H.-J. Freund, H. Behner, B. Bartos, G. Wedler, H. Kuhlenbeck, M. Neumann, Surf. Sci. 180 (1987) 550.
[55] (a) S.J. Choe, H.J. Kang, D.H. Park, D.S. Huh, J. Park, Appl. Surf. Sci. 181 (2001) 265;
(b) S.J. Choe, D.H. Park, D.S. Huh, Bull. Korean Chem. Soc. 21 (2000) 779.
[56] M.H. Nassir, D. Dwyer, J. Vac. Sci. Technol. 11 (4) (1999) 2104.
[57] T.P.St. Clair, S.T. Oyama, D.F. Cox, S. Otani, Y. Ishizawa, R.-L. Lo, K. Fukui, Y. Iwasawa, Surf. Sci. 426 (1999) 187.
[58] (a) C. Zheng, Y. Apeloig, R. Hoffmann, J. Am. Chem. Soc. 110 (1988) 749;
(b) M.L. Turner, P.K. Byers, H.C. Long, P.M. Maitlis, J. Am. Chem. Soc. 115 (1993) 4417.
[59] Vu T.T. Ha, Le V. Tiep, P. Meriaudeau, C. Naceache, J. Mol. Catal. A 181 (2002) 283.